Galvanomagnetic Properties of a Nonellipsoidal, Nonparabolic Band Model. I. Hall Coefficient

R. S. ALLGAIER
U. S. Naval Ordnance Laboratory, White Oak, Silver Spring, Maryland
(Received 8 June 1966; revised manuscript received 1 August 1966)

The factor r, defined in the weak-field Hall-coefficient formula $R_0=r/Ne$, is computed for the case of degenerate statistics using Morrel Cohen's nonellipsoidal, nonparabolic band model. An isotropic scattering time is assumed, but otherwise no approximations are made, despite the complexity of the energy-momentum relationship. Numerical results are presented and discussed for a wide range of values of the two parameters characterizing Cohen's model. The calculations are applied to degenerate p-type SnTe, for which the unusual value $r=0.6$ has been found experimentally. Agreement is obtained using parameter values which correspond to a prolate dumbbell-shaped constant-energy surface. Such a shape had already been inferred from the Shubnikov–de Haas oscillations observed in SnTe.

1. INTRODUCTION

A BAND model has been derived by M. H. Cohen for bismuth[1] in which the constant energy surfaces are not ellipsoidal, and in which the energy-momentum relationship is not parabolic, except along a single momentum axis. The present work presents a derivation of the Hall factor r for the Cohen model, i.e., the factor defined by the formula

$$R_0=r/Ne, \tag{1}$$

which relates the weak-field Hall coefficient R_0 to the carrier concentration N and carrier charge e. A scalar isotropic scattering time is assumed.

The main reason for carrying out the computation was to compare the results with experimental data on SnTe.[2] The basis for applying Cohen's model to SnTe was the general similarity of crystal and band structure between the group V elements As, Sb, and Bi and IV–VI compounds such as PbS, PbSe, PbTe, and SnTe.[3] The Shubnikov–de Haas oscillations recently observed in the magnetoresistance of[4] SnTe have provided a more specific reason for considering the Cohen model.

Aside from possible applications, it also seemed worthwhile to investigate the transport properties of the Cohen model for their own sake. This stemmed from the fact, unusual for so complicated a model, that the integration of the conventional expressions for the transport coefficients may be carried out exactly over a constant energy surface. This analytical property had been discovered earlier for the conductivity integrals,[5] and it seemed likely that it would occur also in the Hall and magnetoconductivity terms.

The more usual situation encountered in nonellipsoidal models is that some kind of an approximation to the exact energy-momentum relationship must be used in order to obtain tractable expressions for the transport coefficients.[6] It then becomes rather difficult to establish that any interesting features emerging from such a computation are an intrinsic property of the exact form of the energy surface rather than a characteristic of the particular approximation used.

It should be emphasized that the exact computation becomes possible *after* the existence of a scalar isotropic scattering time is assumed. Thus, the computation and discussion to follow do not refer to the transport properties of the Cohen surface in the most general sense, but rather to the properties of the isotropic-scattering-time model of the Cohen surface.

2. THE COHEN SURFACE

The IV–VI compounds PbS, PbSe, PbTe, and SnTe all have the NaCl structure,[3] and hence the truncated octahedral Brillouin zone appropriate for the face-centered-cubic crystal lattice. Near their extrema, the conduction and valence bands of the three lead salts are known to consist of four prolate surfaces of revolution, approximately ellipsoidal, with symmetry axes lying along the ⟨111⟩ directions of momentum, and centered on the points where the ⟨111⟩ directions intersect the zone faces.[7] The Shubnikov–de Haas data on p-type SnTe[4] suggest that the top of its valence band also consists of prolate, ⟨111⟩-oriented constant energy surfaces.

The Brillouin zone for Bi resembles that described above, except that it is slightly compressed along one of the ⟨111⟩ directions. This direction then becomes the trigonal axis, while the other three ⟨111⟩ axes correspond closely to the "tilt" directions along which the elongated conduction-band ellipsoids of Bi lie.

Cohen actually derived three types of constant

[1] M. H. Cohen, Phys. Rev. **121**, 387 (1961).
[2] B. B. Houston, R. S. Allgaier, J. Babiskin, and P. G. Siebenmann, Bull. Am. Phys. Soc. **9**, 60 (1964).
[3] M. H. Cohen, L. M. Falicov, and S. Golin, IBM J. Res. Develop. **8**, 215 (1964).
[4] J. R. Burke, R. S. Allgaier, B. B. Houston, J. Babiskin, and P. G. Siebenmann, Phys. Rev. Letters **14**, 360 (1965).
[5] J. R. Dixon and H. R. Riedl, Phys. Rev. **138**, A873 (1965); J. R. Burke, Jr., Ph.D. thesis, Catholic University, 1965 (unpublished). In these cases, the Cohen model was applied to PbTe.
[6] Several examples are discussed in A. C. Beer, *Galvanomagnetic Effects in Semiconductors* (Academic Press Inc., New York, 1963), Chap. 7.
[7] K. F. Cuff, M. R. Ellett, C. D. Kuglin, and L. R. Williams, in *Physics of Semiconductors, Proceedings of the Seventh International Conference, Paris, 1964* (Dunod Cie, Paris, 1964), p. 677.

energy surfaces for Bi. The above-mentioned band structure for SnTe corresponds to Cohen's case (a), which arises when the band edge is located at zone points having rotation plus reflection symmetry. The energy-momentum relation which Cohen obtained in this case is, using his notation,

$$\frac{p_1^2}{2m_1}+\frac{p_3^2}{2m_3}=\frac{1}{\mathcal{E}_g}\left\{\left(\mathcal{E}-\frac{p_2^2}{2m_2}\right)\left(\mathcal{E}+\mathcal{E}_g+\frac{p_2^2}{2m_2'}\right)\right\}. \quad (2)$$

In terms of rhombohedral Bi, axis 1 is parallel to a binary axis, axes 2 and 3 lie in a reflection plane, axis 3 making a small angle (the tilt angle) with the trigonal axis, and axis 2 being the direction along which the substantial elongation of the Bi conduction-band surface occurs.

In cubic SnTe, axis 2 becomes a [111] direction, and axes 1 and 3 lie along [110]- and [112]-type directions. Axis 2 now has acquired threefold rotational symmetry, and this, combined with the limitations imposed by the form of Eq. (2), requires that $m_1=m_3$. Hence, the Cohen surface becomes a surface of revolution about axis 2. Making the substitutions $m_1=m_3=m_t$, $p_1^2+p_3^2=p_t^2$, $m_2=m_l$, $m_2'=m_l'$, $p_2=p_l$, and rearranging Eq. (2) leads to

$$\mathcal{E}=\frac{p_t^2}{2m_t}\frac{1}{1+(\mathcal{E}/\mathcal{E}_g)+(p_t^2/2m_l'\mathcal{E}_g)}+\frac{p_l^2}{2m_l}. \quad (3)$$

Equation (3) differs from an ellipsoidal, parabolic model because of the presence of the energy-gap and "other-band" mass parameters $\mathcal{E}_g$ and m_l', except on the p_l axis (i.e., when $p_t=0$); then it becomes simply $\mathcal{E}=p_l^2/2m_l$. A finite value of $\mathcal{E}_g$ produces a nonparabolic model, regardless of the value of m_l'. A finite value of m_l' leads to a nonellipsoidal constant energy surface, but only if $\mathcal{E}_g$ is also finite.

The computation will be presented in terms of the dimensionless variables $\epsilon=\mathcal{E}/\mathcal{E}_g$, $\mu=m_l/m_l'$, $x^2=p_t^2/m_t\mathcal{E}_g$, and $y^2=p_l^2/m_l\mathcal{E}_g$. These substitutions transform Eq. (3) into

$$\epsilon=\frac{x^2}{2}\frac{1}{1+\epsilon+\mu y^2/2}+\frac{y^2}{2}. \quad (4)$$

Deviations from the parabolic, ellipsoidal model now occur for *nonzero* values of the parameters ϵ and μ.

Figure 1 provides an example of how the cross section of the surface in the x-y plane evolves as the energy increases. Of particular pertinence here is the dumbbell shape, since the SnTe Shubnikov–de Haas data revealed that two extremal cross sections, present when the magnetic field was along a given [111] direction, both increased as the field was turned away from this direction.

As Cohen pointed out, a central minimum in the cross section (and hence in x) will develop when

$$\epsilon>1/(\mu-1), \quad (5)$$

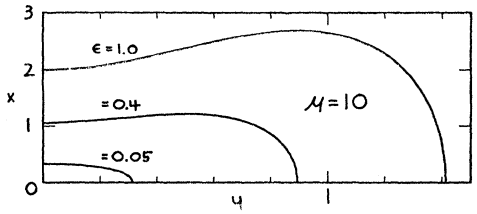

FIG. 1. Examples of the Cohen-model constant energy surfaces: $\mu=10$; $\epsilon=0.05$, 0.4, and 1.0. The intersection of each surface with one quadrant of the x-y plane is shown. The y axis has been lengthened in order to suggest the case of prolate surfaces.

and thus can appear only when $\mu>1$. With increasing ϵ, the two noncentral maximum values of x move outward along the positive and negative branches of the y axis. The value of y at which $x_{\max}$ occurs is related to the extreme values of y (at which $x=0$) by

$$\frac{y^2(x_{\max})}{y^2(x=0)}=\frac{\mu-1}{2\mu}-\frac{1}{2\mu\epsilon}. \quad (6)$$

Thus, $y^2(x_{\max})/y^2(x=0)$ is always less than $\frac{1}{2}$ for finite μ and ϵ. The maximum and minimum cross sections normal to the y axis, $A_{\max}$ and $A_{\min}$, are related by[8]

$$\frac{A_{\max}}{A_{\min}}=1+\frac{[\epsilon(\mu-1)-1]^2}{4\mu\epsilon(1+\epsilon)}. \quad (7)$$

This ratio approaches the limit $(\mu+1)^2/4\mu$ as $\epsilon\to\infty$, and the limit is always greater than $\mu/4$. It should be mentioned that Eqs. (6) and (7) have meaning only when Eq. (5) is valid, and also that Eq. (7) holds for the areas in momentum space, $A=\pi p_t^2$, as well as when $A=\pi x^2$. Similarly, Eq. (6) is also valid when the ratio is expressed in terms of the transverse momentum p_t.

3. OUTLINE OF COMPUTATION

A. Basic Formulas, Simplifications, and Assumptions

It should be emphasized at this point that the contents of Secs. (A), (B), and (C) which follow refer to a single energy surface, or valley. Only in Sec. (D) will the results be combined into expressions for a cubically symmetric arrangement of surfaces, i.e., for a multivalley model.

Comparing an iterative solution of the Boltzmann equation with the formal expression for the current density in terms of the first power of electric field intensity and ascending powers of the magnetic field intensity

$$I_i=\sigma_{ij}E_j+\sigma_{ijk}E_jH_k+\sigma_{ijkl}E_jH_kH_l+\cdots \quad (8)$$

[8] The author is indebted to Claudia C. Evans for pointing out an error in Eq. (7) as originally derived.

leads to the equations[9]

$$\sigma_{ij}=\frac{-2e^2}{h^3}\int\tau\frac{\partial f_0}{\partial\mathcal{E}}\frac{\partial\mathcal{E}}{\partial p_i}\frac{\partial\mathcal{E}}{\partial p_j}dp^3, \tag{9a}$$

$$\sigma_{ijk}=\frac{-2e^3}{h^3}\int\tau\frac{\partial f_0}{\partial\mathcal{E}}\frac{\partial\mathcal{E}}{\partial p_i}\epsilon_{krs}\frac{\partial\mathcal{E}}{\partial p_r}\frac{\partial}{\partial p_s}\left(\tau\frac{\partial\mathcal{E}}{\partial p_j}\right)dp^3, \tag{9b}$$

$$\sigma_{ijkl}=\frac{-2e^4}{h^3}\int\tau\frac{\partial f_0}{\partial\mathcal{E}}\frac{\partial\mathcal{E}}{\partial p_i}\epsilon_{ltu}\frac{\partial\mathcal{E}}{\partial p_t}\frac{\partial}{\partial p_u}\left[\tau\epsilon_{krs}\frac{\partial\mathcal{E}}{\partial p_r}\frac{\partial}{\partial p_s}\times\left(\tau\frac{\partial\mathcal{E}}{\partial p_j}\right)\right]dp^3,$$

$$\cdots. \tag{9c}$$

In the above equations, σ_{ij}, σ_{ijk}, and σ_{ijkl} are the components of the conductivity (in zero magnetic field), Hall, and magnetoconductivity tensors, respectively; summation from 1 to 3 is implied by indices which appear more than once in the same term [namely, j, k, and l in Eq. (8) and r, s, t, and u in Eqs. (9b) and (9c)]; and e is the carrier charge (positive or negative as required), h Planck's constant, τ the scattering time, f_0 the unperturbed Fermi-Dirac distribution, and the ϵ_{abc} are permutation tensors, having zero components except for $\epsilon_{123}=\epsilon_{321}=\epsilon_{312}=+1$ and $\epsilon_{213}=\epsilon_{321}=\epsilon_{132}=-1$.

If the p_l (or y) axis, in terms of which Eqs. (3) and (4) for the Cohen surface were written, is identified with one of the coordinate axes of Eqs. (8) and (9), then the Cohen surface has twofold rotational symmetry about each of its coordinate axes. From this symmetry property alone it follows that the only possible nonzero components among the second- and third-rank terms of Eq. (8) are the σ_{ii}, σ_{iii}, σ_{ijk} (i, j, k all different). From Onsager's principle it follows that $\sigma_{iii}=0$ and $\sigma_{ijk}=-\sigma_{jik}$. If the symmetry axis of the Cohen surface is taken as axis 3 in Eqs. (8) and (9), then axes 1 and 2 are indistinguishable. Consequently, $\sigma_{11}=\sigma_{22}$ and $\sigma_{312}=-\sigma_{321}$. Thus, all the nonzero tensor components of second and third rank may be obtained from the computation of just four of them, for example, from the set

$$\sigma_{11},\ \sigma_{33},\ \sigma_{123},\ \text{and}\ \sigma_{312}. \tag{10}$$

It will be assumed that the scattering time is a scalar function of energy alone. This is a severe restriction, but one which is commonly invoked. Herring and Vogt have shown[10] that results obtained under the assumption of an isotropic scattering time may also be obtained from a scattering time which is the same function of energy, multiplied by a tensor τ_{ii}, if τ_{ii} and m_{ii} are diagonal in the same coordinate system, and if m_{ii} is replaced by an m_{ii}/τ_{ii} of equal value.

When the assumption $\tau=\tau(\mathcal{E})$ is made, all terms involving derivatives of τ cancel. Thus, the τ's appearing at various points in the integrals of Eqs. (9) may be combined in each case into a single factor, not subject to differentiation.

B. Relation between Fermi level and Carrier Concentration

The form of the conductivity and Hall tensor components is greatly simplified by using the relation between carrier concentration and Fermi level. The carrier concentration is given by

$$n=\int_0^\infty[d\mathfrak{N}(\mathcal{E})/d\mathcal{E}]f_0d\mathcal{E}; \tag{11}$$

$\mathfrak{N}(\mathcal{E})$ is the number of states up to energy $\mathcal{E}$, and hence $d\mathfrak{N}(\mathcal{E})/d\mathcal{E}$ is the density of states. The alternative form, obtained through integration by parts, is

$$n=-\int_0^\infty\mathfrak{N}(\mathcal{E})(\partial f_0/\partial\mathcal{E})d\mathcal{E}, \tag{12}$$

and more closely resembles Eqs. (9). The quantity $\mathfrak{N}(\mathcal{E})$ is proportional to the volume contained within the constant energy surface, and this volume turns out to be a very simple function of $\mathcal{E}$. The final result is

$$n=\frac{-2^{9/2}\pi m_t m_l^{1/2}}{3h^3}\int_0^\infty A_n\mathcal{E}^{3/2}\frac{\partial f_0}{\partial\mathcal{E}}d\mathcal{E}, \tag{13}$$

where

$$A_n=1+\epsilon(1+\mu/5). \tag{14}$$

The only difference between Eq. (13) and the corresponding expression for the ellipsoidal, parabolic model having the same m_t and m_l is the presence of the factor A_n. The simplicity of this result occurs because the "correction factor," which enters once for each nonparabolic axis, has the form of a square root of a polynomial, and the Cohen model is nonparabolic in *two* directions.

C. Single-Valley Conductivity and Hall Tensor Components

The computation of the conductivity and Hall tensor components is straightforward but lengthy. Some of the intermediate steps are outlined and discussed in Appendix A. The results for the four independent

[9] Reference 6, Chap. 3, particularly pp. 37–38.
[10] C. Herring and E. Vogt, Phys. Rev. **101**, 944 (1956).

quantities given in Eq. (10) are[11]

$$\sigma_{11}=\frac{ne^2}{m_t}\frac{\int_0^\infty \tau A_{11}\mathcal{E}^{3/2}(\partial f_0/\partial\mathcal{E})d\mathcal{E}}{\int_0^\infty A_n\mathcal{E}^{3/2}(\partial f_0/\partial\mathcal{E})d\mathcal{E}}, \quad (15a)$$

$$\sigma_{33}=\frac{ne^2}{m_l}\frac{\int_0^\infty \tau A_{33}\mathcal{E}^{3/2}(\partial f_0/\partial\mathcal{E})d\mathcal{E}}{\int_0^\infty A_n\mathcal{E}^{3/2}(\partial f_0/\partial\mathcal{E})d\mathcal{E}}, \quad (15b)$$

$$\sigma_{123}=\frac{ne^3}{m_t^2}\frac{\int_0^\infty \tau^2 A_{123}\mathcal{E}^{3/2}(\partial f_0/\partial\mathcal{E})d\mathcal{E}}{\int_0^\infty A_n\mathcal{E}^{3/2}(\partial f_0/\partial\mathcal{E})d\mathcal{E}}, \quad (15c)$$

and

$$\sigma_{312}=\frac{ne^3}{m_t m_l}\frac{\int_0^\infty \tau^2 A_{312}\mathcal{E}^{3/2}(\partial f_0/\partial\mathcal{E})d\mathcal{E}}{\int_0^\infty A_n\mathcal{E}^{3/2}(\partial f_0/\partial\mathcal{E})d\mathcal{E}}, \quad (15d)$$

where

$$A_{11}=(1+2\epsilon)^{-1}\{(3/2)(1+\epsilon)L_1^0-(1/2)[1+\epsilon(1-\mu)]L_1^2-(3/10)\mu\epsilon L_1^4\}, \quad (16a)$$

$$A_{33}=(1+2\epsilon)^{-1}\{[1+\epsilon(1-\mu)]^2L_1^2+(12/5)\mu\epsilon[1+\epsilon(1-\mu)]L_1^4+(12/7)\mu^2\epsilon^2L_1^6\}, \quad (16b)$$

$$A_{123}=(1+2\epsilon)^{-2}\{(3/2)(1+\epsilon)L_2^0-(1/2)[1+\epsilon(1-\mu)]L_2^2-(3/10)\mu\epsilon L_2^4\}, \quad (16c)$$

and

$$A_{312}=(1+2\epsilon)^{-2}\{[1+\epsilon(1-\mu)]^2L_2^2+(12/5)\mu\epsilon[1+\epsilon(1-\mu)]L_2^4+(12/7)\mu^2\epsilon^2L_2^6\}-(1-\mu)\epsilon(1+2\epsilon)^{-3}\{(1+\epsilon)[1+\epsilon(1-\mu)]L_3^2+(3/5)\{2\mu\epsilon(1+\epsilon)-[1+\epsilon(1-\mu)]^2\}L_3^4-(9/7)\mu\epsilon[1+\epsilon(1-\mu)]L_3^6-(2/3)\mu^2\epsilon^2L_3^8\}. \quad (16d)$$

The functions L_α^β are listed and discussed in Appendix B. They depend only on a particular combination of the mass and energy parameters, namely $w=(\mu-1)\epsilon/(1+2\epsilon)$, and an important property of the $L_\alpha^\beta(w)$ is that they all reduce to unity when $w=0$, i.e., when $\mu=1$.

D. Conductivity and Hall Tensor Components for a Cubically Symmetric Multivalley Model

The final step in the computation is to arrange a set of valleys in a cubically symmetric array, transform the tensor components of each valley to the cubic-axis coordinate system, and sum the contributions from all of the valleys. When this is done for an *ellipsoidal, parabolic model* having t valleys, the relationships between the cubic-axis (primed) tensor components and the principal-axis (unprimed) tensor components of *one* of the valleys are found to be[12]

$$\sigma'_{ii}=(t/3)(\sigma_{11}+\sigma_{22}+\sigma_{33})=(t/3)(2\sigma_{11}+\sigma_{33}) \quad (17a)$$

and

$$\sigma'_{ijk}=(t/3)(\sigma_{123}+\sigma_{231}+\sigma_{312})\epsilon_{ijk}=(t/3)(\sigma_{123}+2\sigma_{312})\epsilon_{ijk}, \quad (17b)$$

where i, j, and k are all different, but otherwise arbitrary. Thus, as expected for any cubic model, the conductivity and Hall tensors each contain only one independent component; furthermore, the orientation of the symmetry axes of the valleys relative to the cubic axes does not appear in either result.

The *present calculation* has found the same nonzero tensor components and the same equalities among them as occur in the ellipsoidal, parabolic model. This is to be expected, since both models have the same symmetry. Hence Eqs. (17) also hold for the Cohen model.

The weak-field Hall coefficient is defined as

$$R_0=\frac{\sigma'_{ijk}\epsilon_{ijk}}{\sigma'^2_{ii}}; \quad (18)$$

summation over repeated indices is not implied in this equation. Using the results obtained in Eqs. (13), (15), and (17) then leads to the Hall factor for the Cohen model

$$r=\frac{3K\left\{\int_0^\infty \tau^2A_{123}\mathcal{E}^{3/2}(\partial f_0/\partial\mathcal{E})d\mathcal{E}+2\int_0^\infty \tau^2A_{312}\mathcal{E}^{3/2}(\partial f_0/\partial\mathcal{E})d\mathcal{E}\right\}\left[\int_0^\infty A_n\mathcal{E}^{3/2}(\partial f_0/\partial\mathcal{E})d\mathcal{E}\right]^{-1}}{\left\{\left[2K\int_0^\infty \tau A_{11}\mathcal{E}^{3/2}(\partial f_0/\partial\mathcal{E})d\mathcal{E}+\int_0^\infty \tau A_{33}\mathcal{E}^{3/2}(\partial f_0/\partial\mathcal{E})d\mathcal{E}\right]\left[\int_0^\infty A_n\mathcal{E}^{3/2}(\partial f_0/\partial\mathcal{E})d\mathcal{E}\right]^{-1}\right\}^2}, \quad (19)$$

where $R_0=r/Ne$, $N=tn$ (the total carrier concentration), and $K=m_l/m_t$.

When $\epsilon\to 0$, the Cohen model, Eq. (4), reduces to the ellipsoidal, parabolic model. Then A_n, A_{11}, A_{33},

[11] The results for Eqs. (15a) and (15b) were obtained previously; see Ref. 5.

[12] F. J. Blatt, in *Solid State Physics* (Academic Press Inc., New York, 1957), Vol. 4, p. 283.

TABLE I. Representative values of the Hall factor r for degenerate statistics, for $K=5$ and 25, and for various values of μ and ϵ.

	$K=5$							$K=25$						
$\epsilon=$	0	0.4	1	$\mu=$ 3	10	30	100	0	0.4	1	$\mu=$ 3	10	30	100
0	0.868	0.868	0.868	0.868	0.868	0.868	0.868	0.779	0.779	0.779	0.779	0.779	0.779	0.779
0.3	0.904	0.902	0.899	0.888	0.828	0.580	0.180	0.791	0.790	0.789	0.789	0.810	0.852	0.728
1	0.968	0.962	0.953	0.905	0.654	0.259	0.069	0.821	0.816	0.812	0.811	0.812	0.696	0.357
3	1.033	1.025	1.000	0.847	0.384	0.106	0.030	0.887	0.879	0.870	0.847	0.715	0.405	0.152
10	0.901	0.890	0.838	0.569	0.155	0.036	0.011	1.009	0.999	0.977	0.860	0.469	0.162	0.052
30	0.538	0.529	0.481	0.275	0.057	0.012	0.004	1.023	1.010	0.960	0.703	0.231	0.060	0.018
100	0.213	0.209	0.186	0.096	0.018	0.004	0.001	0.695	0.682	0.625	0.371	0.083	0.019	0.006

A_{123}, and A_{312} all become unity, and the Hall factor, Eq. (19), takes on the familiar form[13]

$$r=\frac{\langle\tau^2\rangle 3K(K+2)}{\langle\tau\rangle^2(2K+1)^2}, \tag{20}$$

where

$$\langle\tau^\gamma\rangle=\frac{\int_0^\infty \tau^\gamma \mathcal{E}^{3/2}(\partial f_0/\partial\mathcal{E})d\mathcal{E}}{\int_0^\infty \mathcal{E}^{3/2}(\partial f_0/\partial\mathcal{E})d\mathcal{E}}. \tag{21}$$

A less simple model might be imagined in which the various A's were not unity, but were all equal to the *same* function of energy, $A(\mathcal{E})$. Then Eqs. (20) and (21) could still be written down, but Eq. (21) would contain $A(\mathcal{E})$ in numerator and denominator. The new complication which appears in the Cohen model is that the integrals in Eq. (19) contain A's which are *different* functions of energy, and they cannot be factored out and separated from a function which depends only on mass anisotropy.

The Hall factor for the Cohen model does simplify considerably in the limiting case of highly degenerate statistics, when $\partial f_0/\partial\mathcal{E}$ becomes a delta function at $\mathcal{E}_F$, the Fermi level. It should be noted that the magnitude of r is then determined only by *mass anisotropy*, since carriers of different energies are not considered, and since it has been assumed that τ is isotropic. In this case, Eq. (19) reduces to

$$r=\frac{3XK(YK+2)}{(2ZK+1)^2}, \tag{22}$$

where $X=A_nA_{312}/A_{33}^2$, $Y=A_{123}/A_{312}$, and $Z=A_{11}/A_{33}$. The simplest case (for nonzero ϵ) occurs when $\mu=1$. Then

$$X=Y=Z=\frac{1+(6/5)\epsilon}{1+(12/5)\epsilon+(12/7)\epsilon^2}, \tag{23}$$

and Eq. (22) becomes

$$r=\frac{3K'(K'+2)}{(2K'+1)^2}, \tag{24}$$

where $K'=XK$. Equation (24) is the same function that occurs in the ellipsoidal, parabolic model, except that the variable is K', which equals K for $\epsilon=0$, but decreases monotonically with increasing ϵ.

When $\mu=0$, the constant energy surfaces in the Cohen model become ellipsoids whose anisotropy changes with changing ϵ. It is interesting to note that the simplest result, Eq. (24), occurs not for $\mu=0$ but for $\mu=1$, despite the fact that in the latter case the constant energy surfaces are *not* ellipsoidal.

With the aid of an IBM-7090 computer, numerical values of L_α^β, A_n, A_{11}, A_{33}, A_{123}, A_{312}, X, Y, and Z were calculated for about 300 combinations of the parameters μ and ϵ having values in the range 0 to 100. In each case, the Hall factor was computed for five values of mass ratio K: 5, 10, 25, 50, and 100. Some selected results are presented in Table I, and copies of the complete results, as well as the FORTRAN IV program, may be obtained from the author.

It is to be emphasized that all the results refer to the case of completely degenerate statistics. The integration over energy has not been carried out.

4. DISCUSSION

It is convenient to discuss the behavior of the Hall anisotropy factor r in terms of three cases: $\mu=1$, <1, and >1. In previous sections it was pointed out that relatively simple results occur when $\mu=1$, and that only when $\mu>1$ can the Cohen surface evolve into a dumbbell shape at finite values of ϵ.

Figures 2(a) and 2(b) present a series of curves of r as a function of ϵ, for various values of μ, and for two mass anisotropy values, $K=10$ and 100. The logarithmic scale at the bottom of each figure is the effective anisotropy parameter $K'(=XK)$, and hence it refers only to the curves for which $\mu=1$. The relation between K' and ϵ, Eq. (23), was used to determine the ϵ scale at the top of each figure. This scale applies to all the curves.

A. Case $\mu=1$

It was established in Sec. 3 that for $\mu=1$, $r(K')$ has the same form as $r(K)$ in the ellipsoidal, parabolic model. From the well-known properties of that function[14] it follows that for $K>1$, $r(\epsilon)$ starts out at $\epsilon=0$

[13] Reference 6, Chap. 8.

[14] See the figure on p. 216 of Ref. 6.

with a value between 0.75 and 1.00 increases gradually as ϵ increases, reaches a maximum of 1.00 when $K'=XK=1$, and then decreases rather rapidly towards zero with further increase in ϵ. In the parallel case of the ellipsoidal, parabolic model, the increase corresponds to a surface which is becoming less prolate, the maximum to a spherical surface, and the decrease to an increasingly more oblate surface.

B. Case $\mu<1$

When $\mu<1$, the distortion of the constant energy surface from an ellipsoidal form is relatively slight. The effect on $r(\epsilon)$ is also modest, leading to curves lying somewhat above the $\mu=1$ curve. The highest curve appears to be the one for $\mu=0$ (ellipsoidal surfaces with energy-dependent elongation). Thus, in contrast to the ellipsoidal, parabolic model, the anisotropy factor may exceed unity over a certain range of ϵ values. This new feature is not particularly important, however, since the maximum $r(\epsilon)$ values are only about 1.03 ($K=10$) and 1.05 ($K=100$).

C. Case $\mu>1$

For $\mu>1$, the behavior of $r(\epsilon)$ is sensitive to the choice of mass anisotropy K. Figure 2(a) illustrates the behavior for a prolate surface of moderate elongation, $K=10$. Except for the possibility of some very slight crossing of curves near $\epsilon=0$, increasing the value of μ always lowers the $r(\epsilon)$ curve. An important feature of the $\mu>1$ case in Fig. 2(a) is that a modest value of μ (e.g., 3 or 4) leads to a curve which does not approach unity for any ϵ, while a substantial portion of it lies in the range 0.5–0.8.

In a rough sense, it may be said that all of the $r(\epsilon)$ curves reflect the behavior of a surface which, as ϵ increases, becomes less prolate, and ultimately oblate. The higher the value of μ, the more rapidly the surface undergoes this transformation. That is why the curve for $\mu=20$, $K=10$ drops so rapidly to small values. In this case the surface quickly acquires a form resembling *two* strongly oblate surfaces connected by a relatively thin neck.

The curves of Fig. 2(b) correspond to a more strongly elongated surface, $K=100$. The behavior of the first few curves, say those for $\mu=0$, 1, and 2, is quite similar to that of the corresponding curves for $K=10$, Fig. 2(a), except that the curves and the ϵ scale are shifted to the right because of the larger K value. But at higher μ values, the curves rise again and become sharply peaked. Their maxima approach and then exceed unity by a significant amount. The explanation for this behavior seems to be that, as ϵ increases, surfaces with a high μ *and* high K go through an intermediate phase in which they resemble two spheres connected by a narrow neck—hence, $r(\epsilon)$ should be close to unity. With further increase in ϵ, the spheres become oblate and, as in the case of the high μ curves for $K=10$, r drops rapidly to small values.

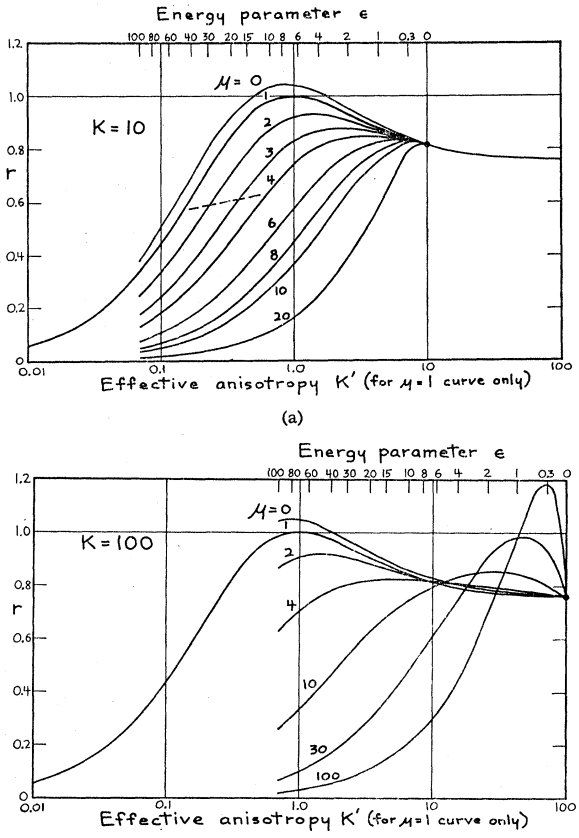

FIG. 2. (a) Hall anisotropy factor r as a function of the energy parameter ϵ, for $K=10$, and for various values of μ. Dashed curve refers to a case (discussed in Sec. 4) in which the parameter μ decreases with increasing ϵ. (b) Same as Fig. (a), except $K=100$.

5. APPLICATION TO SnTe

In p-type SnTe at 77°K, it has been found[2] that $r=0.6\pm10\%$ for carrier concentrations between 5×10^{19} and 1.2×10^{21} cm^{-3}. Degenerate statistics are appropriate for this temperature and range of carrier concentrations. The Shubnikov–de Haas data for[4] SnTe suggest a multivalley model for the valence band consisting of prolate, ⟨111⟩-oriented surfaces.

It is well known that transport theory for prolate, ellipsoidal models (with degenerate statistics) predicts that r will lie in the range between 0.75 and 1. The question is, can distortions of the type introduced by using Cohen's energy-momentum relation change this result significantly? The answer, in general terms, is yes. The $r(\epsilon)$ curves with moderate μ values, corresponding approximately to the kind of dumbbell shapes that can be deduced from the Shubnikov–de Haas data, have values between 0.5 and 0.7 over a substantial range of ϵ; they take on values between 0.7 and 0.9

over a more restricted range of ϵ; they rarely exceed 0.9. To be more specific, the best estimate for the ratio $A_{\max}/A_{\min}$ thus far obtained from the Shubnikov–de Haas data is 1.2. The value $r=0.6$ on the curves for $K=10$, $\mu=2$ and 3 [Fig. 2(a)], corresponds to $A_{\max}/A_{\min}=1.1$ and 1.3, respectively, using Eq. (7).

It is more difficult to interpret the experimental fact that r is nearly constant over a wide range of carrier concentrations.[2] Almost all of the curves in Figs. 2(a) and 2(b) suggest that if $r=0.6$ at a particular value of ϵ, it should decrease rapidly as ϵ (and hence the carrier concentration) increases. This discrepancy becomes less serious if the literal application of the Cohen model to SnTe is abandoned—that is, if the dumbbell shape provided by the model is utilized, but the manner in which the shape evolves as ϵ changes is not used.

The Cohen model implies that all of the constant energy surfaces which constitute one valley are centered about a single point in momentum space. With increasing carrier concentration, the surfaces deform from ellipsoids into dumbbells, and the ratio $A_{\max}/A_{\min}$ increases. It is possible, however, that for SnTe the maximum energy in the valence band occurs along the ⟨111⟩ axes, a short distance inside the zone face.[15] At low enough carrier concentrations the energy surfaces would become pairs of closely spaced ellipsoids. At higher carrier concentrations, these pairs would join to form a dumbbell. Under such conditions, the ratio $A_{\max}/A_{\min}$ would *decrease* with increasing ϵ. In Fig. 2 this would correspond to an $r(\epsilon)$ which cuts across the curves of constant μ in the manner shown by the dashed line. This line could be horizontal, or even acquire a negative slope, if μ decreased rapidly enough with increasing ϵ. In any event, such considerations demonstrate how a relatively constant value of r, much less than unity, could occur within the framework of a model utilizing dumbbell-shaped energy surfaces.

Again it should be emphasized that in this discussion the experimental data have been compared with the transport properties of the Cohen model with a scalar isotropic scattering time assumed.

6. SUMMARY AND CONCLUSIONS

It has been found that the Hall anisotropy factor in p-type SnTe at high carrier concentrations[2] is about 0.6. Shubnikov–de Haas measurements on SnTe[4] suggest that the valence band may consist of prolate, ⟨111⟩-oriented, dumbbell-shaped surfaces. The present calculation demonstrates that it is quite easy to obtain the value $r=0.6$ using Cohen's model,[1] but not as easy to understand its constancy over a wide range of carrier concentrations.

The weak-field Hall factor r in cubic crystals does not differ much from unity if the contributing carriers lie near the edge of a single band, and if the statistics are degenerate. An example is the prolate ellipsoidal, parabolic, multivalley model, for which values of $r<0.8$ are not likely to be encountered. The present computation, utilizing the Cohen model with an isotropic scattering time, may be considered relatively successful in that it can explain the unusual value $r=0.6$ within the framework of a single-band model.

The weak-field magnetoresistance in[16] SnTe exhibits an even more striking departure from that symmetry usually associated with a ⟨111⟩ multivalley model. The analytical expressions for the three weak-field magnetoresistance coefficients in the Cohen model have been worked out[17] and are being programmed. A sequel to the present paper will attempt to determine whether or not the present model is capable of explaining the observed magnetoresistance symmetry as well as the Hall data.

APPENDIX A: COMPUTATION DETAILS

The first step in the computation of the tensor components, Eqs. (9a) and (9b), is to replace the volume element in momentum space by the product of an element of area (on a constant energy surface) and an element of length normal to it:

$$dp^3=dSdp_1=dSd\mathcal{E}/|\mathrm{grad}\mathcal{E}|\,. \tag{A1}$$

Then the element of area is expressed in terms of cylindrical coordinates, with p_l as the symmetry axis (see Fig. 3):

$$dS=p_t d\phi dp_l/\cos\theta=p_t d\phi dp_l/[(\partial\mathcal{E}/\partial p_t)/|\mathrm{grad}\mathcal{E}|]. \tag{A2}$$

Thus,

$$dp^3=d\mathcal{E}p_t d\phi dp_l/(\partial\mathcal{E}/\partial p_t). \tag{A3}$$

The commonly used alternative, to express dS in terms of an area element in the plane normal to p_l, is undesirable in this case because it leads to complicated limits of integration when the dumbbell bulge appears.

Because $\tau=\tau(\mathcal{E})$ only, and because of the reflection symmetry of the Cohen surface in the plane $p_l=0$, the integrals may be put in the form

$$\frac{-2e^{2,3,\text{ or }4}}{h^3}\int_0^\infty \tau^{1,2,\text{ or }3}\frac{\partial f_0}{\partial\mathcal{E}}d\mathcal{E}\int_0^{2\pi}d\phi \times 2\int_0^{p_l(\max)}[\mathcal{I}]p_t dp_l/(\partial\mathcal{E}/\partial p_t). \tag{A4}$$

The integrands $[\mathcal{I}]$ contain various derivatives of $\mathcal{E}$ with respect to p_1, p_2, and p_3. When changed to cylindrical coordinates, they become functions of p_l, p_t, and ϕ, and derivatives of $\mathcal{E}$ with respect to p_l and p_t appear, but not with respect to ϕ, because of the cylindrical symmetry. The expressions for the four independent

[15] L. M. Falicov and S. Golin, Phys. Rev. **137**, A871 (1965).

[16] R. S. Allgaier and B. B. Houston, Bull. Am. Phys. Soc. **7**, 331 (1962); R. S. Allgaier, C. C. Evans, and B. B. Houston, *ibid.* **9**, 646 (1964).

[17] C. C. Evans, M. A. thesis, Wesleyan University, 1965 (unpublished).

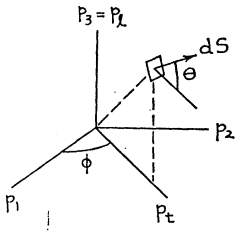

FIG. 3. Procedure for integrating over a constant-energy surface.

tensor components, after they are expressed in the dimensionless coordinates x and y, and after the ϕ integration is carried out, become

$$\sigma_{11}=\frac{-4e^2\pi(m_tm_l^{1/2})\mathcal{E}_g^{3/2}}{h^3m_t}\int_0^\infty \tau\frac{\partial f_0}{\partial\mathcal{E}}d\mathcal{E} \times\int_0^{\sqrt{(2\epsilon)}}\frac{\partial\epsilon}{\partial x}x\,dy, \quad \text{(A5a)}$$

$$\sigma_{33}=\frac{-8e^2\pi(m_tm_l^{1/2})\mathcal{E}_g^{3/2}}{h^3m_l}\int_0^\infty \tau\frac{\partial f_0}{\partial\mathcal{E}}d\mathcal{E} \times\int_0^{\sqrt{(2\epsilon)}}\left[\left(\frac{\partial\epsilon}{\partial y}\right)^2\Big/\left(\frac{\partial\epsilon}{\partial x}\right)\right]x\,dy, \quad \text{(A5b)}$$

$$\sigma_{123}=\frac{-4e^3\pi(m_tm_l^{1/2})\mathcal{E}_g^{3/2}}{h^3m_t^2}\int_0^\infty \tau^2\frac{\partial f_0}{\partial\mathcal{E}}d\mathcal{E} \times\int_0^{\sqrt{(2\epsilon)}}\left(\frac{\partial\epsilon}{\partial x}\right)^2 dy, \quad \text{(A5c)}$$

and

$$\sigma_{312}=\frac{-4e^3\pi(m_tm_l^{1/2})\mathcal{E}_g^{3/2}}{h^3m_tm_l}\int_0^\infty \tau^2\frac{\partial f_0}{\partial\mathcal{E}}d\mathcal{E} \times\int_0^{\sqrt{(2\epsilon)}}\left[\left(\frac{\partial\epsilon}{\partial y}\right)^2\frac{\partial^2\epsilon}{\partial x^2}x\Big/\left(\frac{\partial\epsilon}{\partial x}\right) +\left(\frac{\partial\epsilon}{\partial y}\right)^2-\frac{\partial\epsilon}{\partial y}\frac{\partial^2\epsilon}{\partial x\partial y}x\right]dy. \quad \text{(A5d)}$$

When the derivatives are evaluated using Eq. (4), and x is eliminated by solving the same equation for x and substituting the result into Eqs. (A5), the integrands reduce to a series of terms which are simple, integrable functions of y. After integration, portions of the results are defined in terms of a set of functions $L_\alpha{}^\beta$ (see Appendix B), and when Eq. (13) for the carrier concentration is used to eliminate most of the factors appearing outside the integral signs in Eqs. (A5), the results take on the more compact form of Eqs. (15) and (16).

APPENDIX B: THE FUNCTIONS $L_\alpha{}^\beta$

Aside from coefficients which are functions of ϵ and μ, the integrals appearing in the expressions for the components of the conductivity and Hall tensors all have the form

$$\int_0^{\sqrt{(2\epsilon)}}\frac{y^\beta dy}{(1+gy^2)^\alpha}, \quad \text{(B1)}$$

where $g=(\mu-1)/2(1+2\epsilon)$. Consider first the case $\beta=0$, $\alpha=1$:

$$\int_0^{\sqrt{(2\epsilon)}}\frac{dy}{1+gy^2}=\frac{\tanh^{-1}\sqrt{(-2g\epsilon)}}{\sqrt{-g}}, \quad g<0 \quad \text{(B2a)}$$

$$=\frac{\tan^{-1}\sqrt{(2g\epsilon)}}{\sqrt{g}}, \quad g>0. \quad \text{(B2b)}$$

If these two cases are rewritten as

$$\sqrt{(2\epsilon)}\left[\frac{\tanh^{-1}\sqrt{(-2g\epsilon)}}{\sqrt{(-2g\epsilon)}}\right] \quad \text{(B3)}$$

and

$$\sqrt{(2\epsilon)}\left[\frac{\tan^{-1}\sqrt{(2g\epsilon)}}{\sqrt{(2g\epsilon)}}\right],$$

the expressions inside the square brackets become functions only of $w=2g\epsilon=(\mu-1)\epsilon/(1+2\epsilon)$, reduce to unity when $w=0$, and share the *same* series expansion in the interval $-1<w\leq 1$:

$$[\ ]=1-\tfrac{1}{3}w+\tfrac{1}{5}w^2-\tfrac{1}{7}w^3+\cdots. \quad \text{(B4)}$$

The series expansion for the case $w>1$ follows from the identity $\tan^{-1}\sqrt{(w)}+\tan^{-1}(1/\sqrt{w})=\pi/2$:

$$=\pi/2\sqrt{(w)}-(1/w)[1-\tfrac{1}{3}w^{-1} +\tfrac{1}{5}w^{-2}-\tfrac{1}{7}w^{-3}+\cdots]. \quad \text{(B5)}$$

Since μ and ϵ are non-negative and finite, no other range of w needs to be considered.

If the above case, $\alpha=1$, $\beta=0$, is defined by the symbol $L_1{}^0$ then the general case of Eq. (B1) may be written

$$\int_0^{\sqrt{(2\epsilon)}}\frac{y^\beta dy}{(1+gy^2)^\alpha}=\frac{[\sqrt{(2\epsilon)}]^{\beta+1}}{\beta+1}L_\alpha{}^\beta(w). \quad \text{(B6)}$$

Clearly, all $L_\alpha{}^\beta\to 1$ when $w\to 0$. Also, all $L_\alpha{}^\beta$ depend only on w. This becomes evident when the recursion formulas

$$\int\frac{dy}{(1+gy^2)^\alpha}=\frac{1}{2(\alpha-1)}\frac{y}{(1+gy^2)^{\alpha-1}} +\frac{[2(\alpha-1)-1]}{2(\alpha-1)}\int\frac{dy}{(1+gy^2)^{\alpha-1}} \quad \text{(B7)}$$

and

$$\int\frac{y^\beta dy}{(1+gy^2)^\alpha}=\frac{1}{g}\left[\int\frac{y^{\beta-2}dy}{(1+gy^2)^{\alpha-1}}-\int\frac{y^{\beta-2}dy}{(1+gy^2)^\alpha}\right] \quad \text{(B8)}$$

are used to express the various $L_\alpha{}^\beta$ in terms of $L_1{}^0$.

The results are

$$L_1^2=[3-3L_1^0]/w,$$
$$L_1^4=[(5/3)w-5+5L_1^0]/w^2,$$
$$L_1^6=[(7/5)w^2-(7/3)w+7-7L_1^0]/w^3,$$
$$L_2^0=[(1/2)L_1^0+(1/2)/(1+w)],$$
$$L_2^2=[(3/2)L_1^0-(3/2)/(1+w)]/w,$$
$$L_2^4=[5-(15/2)L_1^0+(5/2)/(1+w)]/w^2,$$
$$L_2^6=[(7/3)w-14+(35/2)L_1^0-(7/2)/(1+w)]/w^3,$$
$$L_3^2=[(3/8)L_1^0+(3/8)/(1+w)-(3/4)/(1+w)^2]/w,$$
$$L_3^4=[(15/8)L_1^0-(25/8)/(1+w)+(5/4)/(1+w)^2]/w^2,$$
$$L_3^6=[7-(105/8)L_1^0+(63/8)/(1+w)-(7/4)/(1+w)^2]/w^3, \quad \text{(B9)}$$

and

$$L_3^8=[3w-27+(315/8)L_1^0-(117/8)/(1+w)+(9/4)/(1+w)^2]/w^4.$$

PHYSICAL REVIEW VOLUME 152, NUMBER 2 9 DECEMBER 1966

R Center in KCl: Electron-Spin-Resonance Studies of the Ground State*

D. C. KRUPKA† AND R. H. SILSBEE‡
Laboratory of Atomic and Solid State Physics and Department of Physics, Cornell University, Ithaca, New York

(Received 23 June 1966)

A calculation of the g tensor is carried out for the ^2E ground state of the R center in KCl. The method employs linear combinations of atomic orbitals as wave functions, made up of F-center $1s$ states orthogonalized to the occupied states of the crystal, and takes into account the dynamical Jahn-Teller effect and the "many-center" nature of the problem. The positive sign of the g shift $\delta g_{\|}$ is correctly predicted, and the magnitude is in reasonable agreement with experiment. From studies of the stress dependence of $\delta g_{\|}$, a value is obtained for the strength of the Jahn-Teller coupling, which is found to be $k^2=3.0\pm0.5$ in the notation of Longuet-Higgins, Öpik, Pryce, and Sack. The effects of random internal strains are found to play an important role, broadening the signal beyond observability at zero applied stress. Estimates of the R-center spin-lattice relaxation rate fall considerably short of the experimental value, for which an upper limit is obtained from saturation plots. Experiments to determine the effect of the presence of the R center on the spin-lattice relaxation rate of the F center indicate that the R center forms a significant channel for F-center relaxation at large R concentrations, and may not be dismissed as a possible relaxation channel at very low R concentrations.

I. INTRODUCTION

IN an earlier publication,[1] the observation of an electron-spin-resonance (ESR) signal identified with the R center in KCl was reported. The results of the initial experiments gave considerable support to the van Doorn model[2] of the R center: three F centers in an equilateral triangular arrangement with a ⟨111⟩ symmetry axis (see Fig. 1). Subsequent work by Silsbee[3] (hereinafter referred to as I), and Seidel, Schwoerer, and Schmid[4] has further demonstrated the validity of the model. The purpose of this paper is to describe additional ESR experiments on this system, and to set up a theory to explain the main features of the resonance. This work complements the optical studies of I and draws on the theoretical framework set up in that paper

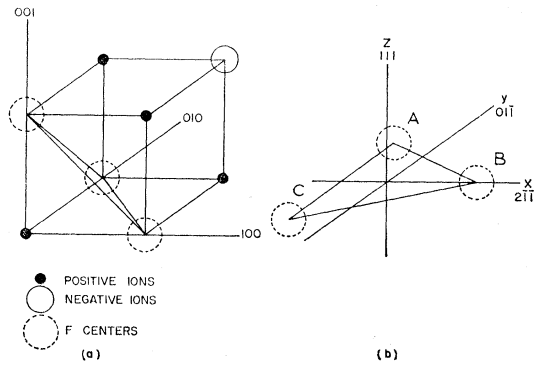

FIG. 1. The van Doorn model of the R center. (a) Ionic configuration. (b) Local axes for a [111] R center.

* Work supported by the U. S. Atomic Energy Commission.
† Present address: Clarendon Laboratory, University of Oxford, Oxford, England.
‡ On leave 1965–66, Swiss Federal Institute, Zürich, Switzerland.
[1] D. C. Krupka and R. H. Silsbee, Phys. Rev. Letters **12**, 193 (1964).
[2] C. Z. van Doorn, Philips Res. Rept. Suppl. 4, (1962).
[3] R. H. Silsbee, Phys. Rev. **138**, A180 (1965).
[4] H. Seidel, M. Schwoerer, and D. Schmid, Z. Physik **182**, 398 (1965).